ELSEVIER

Solid State Ionics 118 (1999) 355–363

SOLID STATE IONICS

Defect, protons and conductivity in brownmillerite-structured $Ba_2In_2O_5$

C.A.J. Fisher[a,*], M.S. Islam[b]

[a]*Department of Materials, University of Oxford, Parks Road, Oxford OX1 3PH, UK*
[b]*Department of Chemistry, University of Surrey, Guildford GU2 5XH, UK*

Received 5 December 1997; accepted 9 February 1998

Abstract

Defect energetics of $Ba_2In_2O_5$ have been investigated by atomistic modelling techniques with emphasis on different modes of conductivity. Oxygen Frenkel pairs were found to be the most energetically favourable intrinsic defects and are responsible for oxide ion conductivity in the orthorhombic structure. Formation energies of electronic species suggest that $Ba_2In_2O_5$ will oxidize readily to produce positive holes. Energies of proton incorporation reveal that $Ba_2In_2O_5$ should also exhibit reasonable proton conductivity in moist atmospheres.

Keywords: Atomistic simulation; Barium indate; Brownmillerite; Oxide ion conductivity; Proton

1. Introduction

Brownmillerite-structured oxides, $A_2B_2O_5$, have been attracting attention recently as possible fast oxide ion conductors for use in oxygen sensors, solid oxide fuel cells, separation membranes and other electrochemical devices [1–5]. Named for the mineral brownmillerite, Ca_2FeAlO_5 [6], the structure of these compounds is a derivative of the perovskite structure, AMO_3, in which the tetravalent M cations in a 2:4 perovskite (or trivalent A cations in a 3:3 perovskite) have been completely substituted by cations one less in valency. To maintain charge balance, one-sixth of the anions are removed [1] and the brownmillerite structure responds to the high concentration of vacancies by ordering them in parallel rows, resulting in the alternating sequence of octahedral and tetrahedral layers shown in Fig. 1. Because this ordering effectively traps the vacancies at fixed positions, they do not contribute to rapid ion conductivity at moderate temperatures. Furthermore, these vacancies are not normally occupied and thus must be treated as interstitial sites in the brownmillerite structure.

Goodenough et al. [2] first stimulated interest in brownmillerites for high oxygen flux applications by showing that above a transition temperature, $T_t \approx 925$°C, $Ba_2In_2O_5$ exhibits a dramatic increase in electrical conductivity as the 'trapped' oxygen vacancies become partially disordered [7]. On further heating, the vacancies become completely disordered so that the structure reverts to that of a highly defective cubic perovskite [4]. Attempts to stabilize the disordered phase at lower temperatures by selec-

*Corresponding author, Synergy Ceramics Laboratory, 2-4-1 Mutsuno, Atsuta-ku, Nagoya 456, Japan. Tel: +81-52-871-8815; fax: +81-52-871-8826; e-mail: fisher@mxj.mesh.ne.jp

0167-2738/99/$ – see front matter
PII: S0167-2738(98)00391-9

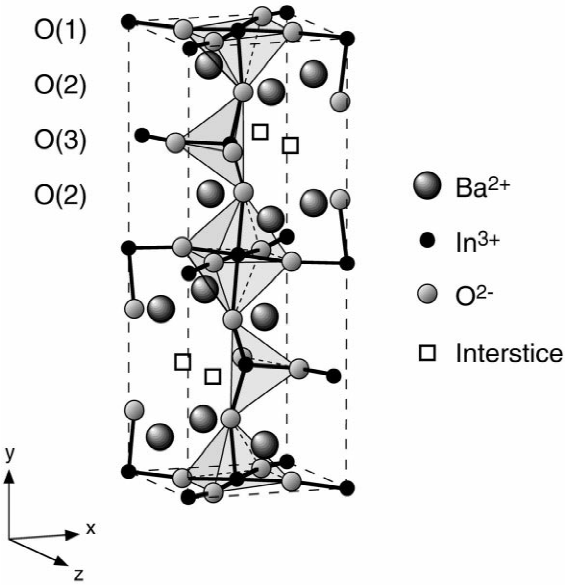

Fig. 1. The unit cell of Ba_2InO_5 showing interstitial sites (open squares) and the layers of crystallographically distinct oxygen sites. Indium ions sit at the entres of oxygen octahedra and tetrahedra, while the larger barium cations occupy the open spaces between O(2) ions.

tive doping of A and/or B sites have met with some success [5,8–11], but oxide ion conductivities are not significantly improved compared to fluorite-structured oxides such as yttria-stabilized zirconia [1]. In addition, $Ba_2In_2O_5$ has been reported to display both electronic conductivity under variable redox conditions [2,3] and proton conductivity due to water incorporation in its low temperature form [12,13]. A review of results of experimental studies of ionic conductivity in brownmillerite and related oxides has been compiled by Kendall et al. [14].

Computer simulation studies are useful tools for analysing defect structures and ion migration at the atomic level. Simulation techniques have been successfully applied to a number of $LaMO_3$ perovskite-related compounds [15–18], including the high-temperature cuprate superconductors [19] and, more recently, the fast ion conductor, doped $LaGaO_3$ [20]. In the current work, we extend a previous computer simulation study [21] to combine an analysis of proton incorporation with that of ionic and electronic defects in $Ba_2In_2O_5$.

2. Simulation methods

2.1. Interatomic potentials and perfect crystal calculations

The atomistic simulation technique employed is based on the Born model of polar solids, in which forces are assumed to be two-body and a function of the distance between ions, *r*, only. Interatomic potentials in the form of Eq. (1) were used to describe atomic interactions. These consist of a long-range Coulombic term and a short-range term of the Buckingham type to approximate electron cloud interactions such as Pauli repulsion and dispersion forces:

$$\phi_{ij}(r) = \frac{q_i q_j}{r_{ij}} + A_{ij} \exp\left(\frac{-r_{ij}}{\rho_{ij}}\right) - \frac{C_{ij}}{r_{ij}^6} \quad (1)$$

where *r* is the distance between ions of species *i* and *j* with charges q_i and q_j, respectively, and A_{ij}, ρ_{ij} and C_{ij} are parameters for each interaction pair.

Electronic polarization effects were taken into account via the shell model [22], which treats each ion in terms of a massive core of charge *X* connected by a harmonic spring to a massless shell of charge *Y*. *X* and *Y* were chosen such that their sum was equal to the formal valence of the ion. Coupling between the short-range forces and polarization by the surrounding lattice was included by making the non-Coulombic forces act only between shells. All simulations were performed using the GULP code [23].

The short-range potential parameters and shell model parameters were first taken from studies of related oxides [17,19,24]. These were adjusted to reproduce the orthorhombic lattice parameters reported by Kuramochi et al. [8], assuming $Ba_2In_2O_5$ to be isostructural with $Ca_2Fe_2O_5$ [25], since no refinement of the orthorhombic structure of $Ba_2In_2O_5$ is yet available [14]. The final parameters are listed in Table 1. The bond distances/angles and properties of the simulated structure calculated using these parameters are given in Table 2 and Table 3, respectively. The small deviation in lattice parameters from the experimentally determined values provides confidence that the model is an accurate representation of brownmillerite $Ba_2In_2O_5$.

Table 1
Interatomic potential parameters for $Ba_2In_2O_5$

(i) Short-range

Interaction	A (eV)	ρ (Å)	C (eV Å^6)
Ba^{2+}–O^{2-}	2096.8	0.3522	8.0
In^{3+}–O^{2-}	1495.6	0.3310	4.325
O^{2-}–O^{2-}	22764.3	0.149	171.983

(ii) Shell model[a]

Species	Y (e)	k (eV Å^{-2})
Ba^{2+}	1.848	29.1
In^{3+}	−6.1	1680.0
O^{2-}	−2.24	42.0

[a]Y and k refer to the shell charge and harmonic force constant, respectively.

2.2. Defect crystal calculations

The potentials developed above were used in calculations of defect formation and migration energies based on the Mott–Littleton approximation in which ions in an inner region surrounding the defect are treated explicitly while the remainder of the crystal is treated by quasi-continuum methods [26]. This method allows local relaxation around the defect to be modelled so that the crystal is not considered simply as a rigid lattice.

The simplest defects considered were intrinsic, or thermal, defects such as vacancies and interstitials which combine as Schottky or Frenkel pairs in real materials. This was followed by estimating oxygen migration paths and energies by placing single oxide ions in 'transition' states between normal anion positions. The transition state was assumed to be the saddle-point of the energy surface between initial and final sites of an ion migrating between adjacent sites.

Next, various charged defects on different crystal-

Table 2
Calculated bond distances and bond angles in the unit cell of $Ba_2In_2O_5$[a]

Separation	Distance (Å) or angle (°)	Separation	Distance (Å) or angle (°)
Ba polyhedron			
Ba–O(1)	2.796 [1]	Ba–O(2)	3.102 [1]
Ba–O(1)	2.759 [1]	Ba–O(2)	2.762 [1]
Ba–O(1)	2.761 [1]	Ba–O(2)	2.931 [1]
Ba–O(1)	2.728 [1]	Ba–O(3)	2.749 [1]
		Mean Ba–O	2.824
In(1) polyhedron			
In(1)–O(1)	2.126 [2]	O(1)–O(1)	2.969 [2]
In(1)–O(1)	2.129 [2]	O(1)–O(1)	3.049 [2]
In(1)–O(2)	2.285 [2]	O(2)–O(1)	3.059 [2]
Mean In(1)–O	2.180	O(2)–O(1)	3.113 [2]
		O(2)–O(1)	3.133 [2]
O(1)–In(1)–O(1)	88.5	O(2)–O(1)	3.182 [2]
O(1)–In(1)–O(1)	91.5		
O(1)–In(1)–O(2)	87.7	O(1)–In(1)–O(2)	89.6
O(1)–In(1)–O(2)	92.3	O(1)–In(1)–O(2)	90.4
In(2) polyhedron			
In(2)–O(2)	1.961 [2]	O(2)–O(2)	4.569 [1]
In(2)–O(3)	1.944 [1]	O(2)–O(3)	3.024 [2]
In(2)–O(3)	1.960 [1]	O(2)–O(3)	3.077 [2]
Mean In(1)–O	1.955	O(3)–O(3)	3.138 [1]
O(2)–In(2)–O(2)	137.4	O(2)–In(2)–O(3)	103.4
O(2)–In(2)–O(3)	101.5	O(3)–In(2)–O(3)	107

[a]Square parentheses indicate number of equivalent distances per polyhedron.

Table 3
Calculated properties of a perfect crystal of $Ba_2In_2O_5$

Property	$Ba_2In_2O_5$
Lattice energy (eV formula unit^{-1})	−207.96
Unit cell parameters (Å)[a]	
a	6.08 (6.09)
b	16.40 (16.79)
c	5.94 (5.88)
Elastic constants (10^{11} dyne cm^{-2})	
c_{11}	20.49
c_{12}	11.92
c_{13}	6.28
c_{33}	7.25
c_{44}	5.37
c_{66}	6.97
Dielectric constants	
$<\varepsilon_s>$	7.28
$<\varepsilon_\infty>$	1.98

[a]Experimental values in parentheses.

lographic sites were treated in order to calculate energies of possible redox reactions. In the last part of the study, protons associated with each of the oxygen sites labelled in Fig. 1 were considered. For these calculations, an attractive Morse potential was used to model the O–H interaction:

$$\phi_{O-H}(r) = D\{1 - \exp[-\beta(r - r_0)]\}^2 \quad (2)$$

where D is the bond dissociation energy, r_0 is the equilibrium bond distance and is a function of the slope of the potential energy well. The values used for these parameters were developed by Saul et al. [27] listed in Table 4. Charges on the hydroxyl species were distributed across both ions to give an overall charge of −1 and the correct dipole moment of the OH group. Our analysis follows closely that of Cherry et al. [15] for other perovskite oxides.

Table 4
Morse potential parameters for the O–H interaction

D (eV)	β (Å^{-1})	r_0 (Å)
7.0525	2.1986	0.9845

3. Results and discussion

3.1. Atomic defects and oxygen migration

Calculations of the energies of isolated point defects (vacancies on each of the atom sites and interstitials at various positions throughout the crystal) were performed by the Mott-Littleton method using a cut-off distance for the inner defect region of 7.5. These energies were combined with the calculated lattice energy to give the Schottky and Frenkel energies listed in Table 5. No indium Frenkel energy is reported because wherever an interstitial indium ion was placed, the structure became unstable and no minimum energy could be found.

The lowest intrinsic defect energy of Table 5 is for oxygen Frenkel pairs formed by an oxygen ion from the O(1) site jumping to an interstitial site [21]. The calculated defect energy of 0.91 eV is in close agreement with the value of 0.84 eV reported by Zhang et al. [3]. The low Frenkel energy suggests that the defect concentration at intermediate temperatures in the brownmillerite structure will be significant. The vacancies produced in this manner can thus explain the low temperature conductivity observed experimentally [2–5,7,8], with displaced oxide ions readily accommodated on the open interstitial sites in the tetrahedral layer. A similar mechanism of ionic conductivity is observed in undoped fluorite phases of ThO_2 and CeO_2 [28]. A possible explanation for the sudden transition of $Ba_2In_2O_5$ to a fast oxide ion conductor is that as the concentration of Frenkel defects increases, the coordination environments of the O(1) and O(3) sites become similar until a critical concentration of defects is reached. At the transition temperature, the defect concentration is

Table 5
Calculated energies of atomic defects in $Ba_2In_2O_5$

Type	Defect equilibrium[a]	Energy (eV/defect)
Ba Frenkel	$Ba_{Ba}^{\times} \leftrightarrow V_{Ba}'' + Ba_i^{\cdot\cdot}$	5.68
O Frenkel	$O_O^{\times} \leftrightarrow V_O^{\cdot\cdot} + O_i''$	0.91
Schottky	$2Ba_{Ba}^{\times} + 2In_{In}^{\times} + 5O_O^{\times} \leftrightarrow 2V_{Ba}'' + 2V_{In}''' + 5V_O^{\cdot\cdot} + Ba_2In_2$	3.56

[a]Kröger–Vink notation used.

sufficient to make the O(1) and O(3) sites indistinguishable; the 'ordered' vacancies released in this manner can diffuse rapidly through the material, at least in these two planes. However, since this treatment ignores structural dynamic effects, the situation may be more complex, as discussed by Adler et al. [4].

Oxygen diffusion in $Ba_2In_2O_5$ below the order–disorder temperature is possible because of the presence of oxygen Frenkel defects. The precise migration mechanism or pathway controlling oxide ion transport, however, is still not certain. Since vacancies on the O(1) site were shown to be more energetically favourable, two possible diffusion pathways might be via O(1) sites in the octahedral layers or interstitial sites in the tetrahedral layers.

Ordering of the low temperature brownmillerite phase into octahedral and tetrahedral layers results in an orthorhombic unit cell with different bond distances between O(1) sites in the [100] and [001] directions. The migration enthalpies calculated for motion in these two directions, as well as diffusion via the interstitial sites in the tetrahedral layer, are listed in Table 6.

These results show that jumps between the shortest distance in the octahedral layers have the lowest activation energy, although activation energies in the other directions are not much greater. A slight anisotropy in oxide ion diffusion is therefore expected in favour of the [001] direction in single crystals of $Ba_2In_2O_5$. The activation enthalpy of 1.2 eV is also consistent with experimentally determined energies of 1.0 eV taken from conductivity measurements below T_t [3]. As mentioned above, at higher temperatures the concentration of interstitial oxide ions in the tetrahedral layer will increase until the coordination environments of O(3) ions approximate those of the O(1) layer, so that the activation energy for diffusion in this layer should approach that of O(1) vacancies.

Table 6
Migration energies of oxygen vacancies in $Ba_2In_2O_5$

Jump path	Migration energy ΔH_m (eV)	Distance (Å)
Octahedral [100]	1.47	3.05
Octahedral [001]	1.21	2.97
Tetrahedral [001]	1.34	2.97

3.2. Redox reactions

$Ba_2In_2O_5$ has been reported to be a mixed ionic/electronic conductor in its low temperature, ordered form, displaying *p*-type conductivity at high oxygen partial pressures and *n*-type conductivity in the low partial pressure regime [3]. Defect calculations for several redox reactions leading to deviations from stoichiometry were considered in order to determine which mechanisms are likely to be responsible for introduction of electronic components (holes or electrons) to the total conductivity of the material.

For oxidation, three possible reactions can occur:

$$\frac{1}{2}O_{2(g)} \rightarrow O_i'' + 2h^{\cdot} \quad (3)$$

to give an oxygen excess material, or alternatively

$$\frac{1}{2}O_{2(g)} + Ba_{Ba}^{\times} \rightarrow V_{Ba}'' + 2h^{\cdot} + BaO \quad (4)$$

and/or

$$\frac{1}{2}O_{2(g)} + \frac{2}{3}In_{In}^{\times} \rightarrow \frac{2}{3}V_{In}''' + 2h^{\cdot} + \frac{1}{3}In_2O_3 \quad (5)$$

to give a metal deficient material. In the case of reduction, only one reaction mechanism was considered:

$$O_O^{\times} \rightarrow V_O^{\cdot\cdot} + \frac{1}{2}O_{2(g)} + 2e' \quad (6)$$

giving an oxygen deficient material, since in Section 3.1 introduction of cation interstitials was found to be a less favourable process.

Our approach for electronic defects in $Ba_2In_2O_5$ follows that used for $LaMO_3$ perovskites [18] and the cuprate superconductors [19], in which the hole centres are modelled as In^{4+} or O^- and the electron centres as In^{2+} or In^+. These electronic defects (or small polarons) were placed on various sites in the brownmillerite structure and the defect energies calculated.

For oxidation, the lowest polaron energy was found for a hole on the O(1) site, i.e. O^-. For reduction, the lowest energy was found for the In^+ ion. When combined with the corresponding interstitial/vacancy energies, along with standard values for the electron affinity and dissociation energy of oxygen and ionization energies of indium, these

Table 7
Calculated energies of electronic defects

Redox reaction	Energy (eV/electron)
Oxidation	
Eq. (3)	2.22
Eq. (4)	4.02
Eq. (5)	4.20
Reduction	
Eq. (6)	4.30

defect energies gave the reaction energies shown in Table 7.

The results show that oxidation most likely occurs via incorporation of oxygen at interstitial sites in the tetrahedral layer (Eq. (3)). The oxidation energy of 2.22 eV is sufficiently low that *p*-type conductivity is expected to occur in mildly oxidizing environments. The higher reduction energy shows that $Ba_2In_2O_5$ is more resistant to reduction than oxidation, and the value of 4.30 eV/electron can be compared to that of 3.5 eV calculated by Zhang et al. using a defect chemistry model [3]. However, to derive a quantitative relationship between oxygen partial pressure and defect concentration, entropic effects need to be included, which is beyond the scope of the current 0 K calculations.

3.3. Proton incorporation

Mobile protons are introduced into oxide materials typically by treatment in water vapour; the protonic defect is described as a hydroxyl group as the proton is closely associated with an oxygen ion. In acceptor doped perovskites, such as $BaCeO_3$ [29], water incorporation can be described by the following reaction, whereby oxygen vacancies are filled by hydroxyl ions:

$$H_2O_{(g)} + V_O^{\cdot\cdot} + O_O^{\times} \rightarrow 2OH_O^{\cdot} \quad (7)$$

The precise process for water incorporation in undoped Ba_2InO_5 and other brownmillerites, however, is less clear, since they contain unoccupied interstitial sites (also referred to as structural oxygen vacancies, which we represent here by the notation $V_i^{\times}$). As well as the hydroxyl group occupying a lattice vacancy (present as an oxygen Frenkel defect) according to Eq. (7), in brownmillerites another possible mechanism is the accommodation of a hydroxyl group at a structural vacancy (interstitial site), with the proton associating with an interstitial oxygen present as a Frenkel defect:

$$H_2O_g + V_i^{\times} + O_i'' \rightarrow 2OH_i' \quad (8)$$

Furthermore, if the oxygen Frenkel reaction (Table 5) is added to Eq. (7), we obtain the reaction suggested by Norby and Larring [30], in which water is incorporated into brownmillerite oxides as protons and oxygen interstitials:

$$H_2O_{(g)} + 2O_O^{\times} + V_i^{\times} \rightarrow 2OH_O^{\cdot} + O_i'' \quad (9)$$

It should be noted, however, that whereas Norby and Larring consider the gaseous water molecule to decompose into an oxygen ion and two protons, here we only consider the water molecule to decompose into a hydroxyl ion and proton [15], so that Eq. (9) occurs in two steps: an oxygen ion first jumps into an interstitial site and then the incoming hydroxyl ion occupies the resultant lattice vacancy, with the free proton associating with another lattice oxygen ion.

The fourth possible incorporation mechanism we consider is the case involving a Frenkel pair where hydroxyl groups occupy both an oxygen vacancy and an interstitial site:

$$H_2O_{(g)} + V_O^{\cdot\cdot} + O_i'' \rightarrow OH_O^{\cdot} + OH_i' \quad (10)$$

Evidence of which site hydroxyl ions prefer in $Ba_2In_2O_5$ has not been reported thus far. However, this is not surprising since the investigation and discussion of such species in undoped oxygen-deficient materials is rather limited. Moreover, the structure of fully hydrated $Ba_2In_2O_5$ has not been studied in detail.

Following our previous work on protons in perovskite oxides [15], we have attempted to examine the energetics of the above reactions in $Ba_2In_2O_5$, although without taking into account entropy terms. An isolated hydroxyl group was placed in vacancies on each of the oxygen sublattice sites, with the proton oriented in different directions, as well as on interstitial sites in the tetrahedral layer, and the structure relaxed according to the Mott-Littleton method in order to determine the defect energy. The lowest defect energy for hydroxyl groups placed on

lattice sites was found for the O(1) site. Compared to the different oxygen sublattice sites, the difference in defect energies between interstitial hydroxyl ions at different structural vacancies were relatively small. The calculated water incorporation energies, E_{H_2O}, of the overall reactions based on these values are listed in Table 8.

Owing to the approximations in the model used, we must be cautious in giving firm conclusions. Nevertheless, the results suggest that incorporation of hydroxyl ions on both interstitial and Frenkel vacancy sites is energetically viable. For Eq. (7), Eq. (8) and Eq. (10) to be possible, however, Frenkel defects must be present. If the oxygen Frenkel energy (1.82 eV) is added to each equation, the water incorporation energies of Eq. (8) and Eq. (10) alone are exothermic (−0.31 and −1.01 eV, respectively). This indicates that simultaneous occupancy of interstitial and lattice oxygen sites by protons from a single water molecule is the most favourable mechanism. However, one must consider that having both defects of a Frenkel pair contributing to the same reaction simultaneously is unlikely and may mean that this mechanism does not occur as a simple single-step process.

The lower energy of Eq. (10) suggests that water incorporation involves the creation of a mixture of $OH_O^{\cdot}$ and OH_i' defects, that is hydroxyl ions on both lattice and interstitial sites. The negative value accords with observation as it is known that this material readily takes up water, with dissolution favoured by decreasing temperatures. Indeed, a recent study found that hydration of $Ba_2In_2O_5$ below 300°C results in an exothermic transition to a new hydrate-like structure of composition $Ba_2In_2O_5 \cdot H_2O$ [13]. Our result is also consistent with the conductivity and EMF measurements of Zhang and Smyth [12] who propose that the proton formation mechanism is by incorporation of H_2O into oxygen vacancies – whether structural or thermal is not made clear – for which they derived a corresponding enthalpy of −0.90 eV.

Table 8
Calculated proton incorporation energies

Incorporation mechanism	E_{H_2O} (eV)
Eq. (7)	≈1.72
Eq. (8)	≈2.13
Eq. (9)	0.09
Eq. (10)	≈2.83

The predicted defect structure and orientation of the OH^- group on an interstitial site is illustrated in Fig. 2. The proton is most stable when pointing towards on O(1) ion in the octahedral layer, almost parallel to the *y* axis. The presence of the hydroxyl ion distorts the tetrahedral layer oxygen sublattice so that the structure becomes more like that of the octahedral layer, although the straightening of the tetrahedral O(2)-In-O(2) bonds near to the interstitial hydroxyl ion, as well as the decrease in the O(3)-In-O(3) bond angle, is not as great as for a single oxygen interstitial in the same position. The O-H bond length is 0.955 Å. Fig. 3 shows the orientation

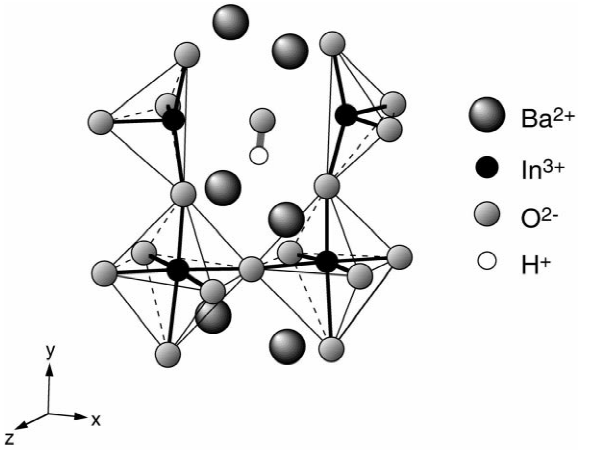

Fig. 2. Orientation of O–H pair at interstitial site in $Ba_2In_2O_5$.

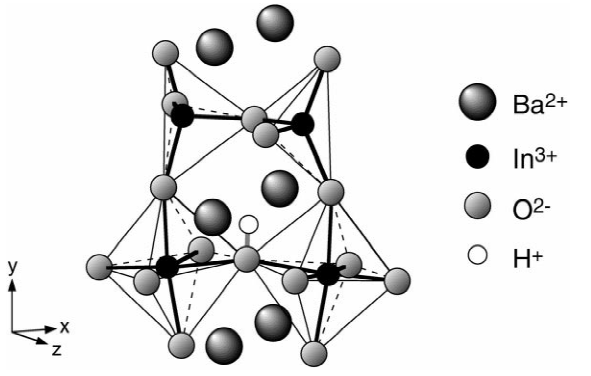

Fig. 3. Orientation of O–H pair occupying O(1) vacancy in $Ba_2In_2O_5$.

of a hydroxyl group on an O(1) site, with the proton directed towards an O(3) ion in the tetrahedral layer. The presence of the proton causes the In-O(1)-In triplet between the octahedra to bend further, as the proton of the OH^- group is pulled towards the O(3) ion. The O-H bond length is the same as for the interstitial hydroxyl ion.

We can also use the energy values from Table 8 to consider the proton exchange reaction between lattice and interstitial oxygen ions:

$$OH_O^{\cdot} + O_i'' \rightarrow OH_i' + O_O^{\times} \quad (11)$$

This reaction can be obtained by subtracting both Eq. (10) and the oxygen Frenkel reaction from Eq. (8), giving a value of -1.10 eV. This suggests that the proton is more stable associated with an oxygen ion on an interstitial site, and will preferentially diffuse from an octahedral oxygen to an interstitial oxygen in the tetrahedral layer. Indeed, Eq. (8), which involves formation of two hydroxyl ions in interstitial positions, has the lowest energy per Frenkel defect of all four mechanisms considered.

The results of this study that the incorporation of water and protonic defects in brownmillerite oxides involves occupancy of interstitial sites (i.e. structural vacancies) in the tetrahedral layers. Furthermore experimental investigation, ideally by in situ characterization, is warranted in order to test these predictions. Ultimately we envisage using these techniques to understand the relation between hydroxyl groups and the order-disorder transition of the oxygen sublattice, as well as determining ways of exploiting the protonic conductivity of this material.

4. Conclusions

Atomistic computer modelling techniques were used to investigate the defect and proton energetics and oxide ion transport mechanisms of $Ba_2In_2O_5$. The simulations showed that oxygen Frenkel pairs are the dominant intrinsic defect in the low temperature phase, with a preference for oxide ion diffusion via these defects in the [001] direction. $Ba_2In_2O_5$ was also predicted to be more resistant to reduction than to oxidation, with reduction involving removal of oxygen from octahedral layers and oxidation involving the insertion of oxide ions into interstitial sites. Incorporation of hydroxyl ions was found to be a favourable process in moist atmospheres, so that $Ba_2In_2O_5$ is expected to exhibit proton conductivity. These findings are in good agreement with results from experimental studies reported so far.

Acknowledgements

The authors are grateful to the Royal Society for supporting C.A.J.F. during this work. Simulations were performed in the Materials Modelling Laboratory (MML) of the Dept. of Materials, Oxford. Thanks are also extended to T. Norby of the University of Oslo for helpful discussions on proton incorporation in oxides.

References

[1] B.C.H. Steele, Mater. Sci. Eng. B 13 (1992) 79.
[2] J.B. Goodenough, J.E. Ruiz-Diaz, Y.S. Zhen, Solid State Ionics 44 (1990) 21.
[3] G.B. Zhang, D.M. Smyth, Solid State Ionics 82 (1995) 161.
[4] S.B. Adler, J.A. Reimer, J. Baltisberger, U. Werner, J. Am. Chem. Soc. 116 (1994) 675.
[5] C.A.J. Fisher, B. Derby, R.J. Brook, Br. Ceram. Proc. 56 (1996) 25.
[6] A.A. Colville, S. Geller, Acta Cryst. B 27 (1971) 2311.
[7] T.R.S. Prasanna, A. Navrotsky, J. Mater. Res. 8 (1993) 1484.
[8] H. Kuramochi, T. Mori, H. Yamamura, H. Kobayashi, T. Mitamura, J. Ceram. Soc. Jpn. 102 (1994) 1159.
[9] J.B. Goodenough, Solid State Ionics 94 (1997) 17.
[10] A. Manthiram, J.F. Kuo, J.B. Goodenough, Solid State Ionics 62 (1993) 225.
[11] J.B. Goodenough, A. Manthiram, P. Paranthaman, Y.S. Zhen, Solid State Ionics 52 (1992) 105.
[12] G.B. Zhang, D.M. Smyth, Solid State Ionics 82 (1995) 153.
[13] T. Schober, J. Friedrich, F. Krug, Solid State Ionics 99 (1997) 9.
[14] K.R. Kendall, C. Navas, J.K. Thomas, H.-C. zur Loye, Solid State Ionics 82 (1995) 215.
[15] M. Cherry, M.S. Islam, J.D. Gale, C.R.A. Catlow, J. Phys. Chem. 99 (1995) 14614.
[16] M.S. Islam, M. Cherry, Solid State Ionics 97 (1997) 33.
[17] M. Cherry, M.S. Islam, C.R.A. Catlow, J. Solid State Chem. 118 (1995) 125.
[18] M.S. Islam, M. Cherry, L.J. Winch, J. Chem. Soc., Fara. Trans. 92 (1996) 479.
[19] M.S. Islam, L.J. Winch, Phys. Rev. B 52 (1995) 10510.
[20] M.S. Khan, M.S. Islam, D. Bates, submitted to J. Phys. Chem. B. 102 (1998) 3099.

[21] C.A.J. Fisher, M.S. Islam, R.J. Brook, J. Solid State Chem. 128 (1997) 137.
[22] B.J. Dick, A.W. Overhauser, Phys. Rev. 112 (1958) 90.
[23] J.D. Gale, GULP (General Utility Lattice Programme), Royal Institution, 1993.
[24] R.W. Grimes, private communication.
[25] A.A. Colville, Acta Crystall. B 26 (1970) 1469.
[26] C.R.A. Catlow, Solid State Ionics 8 (1983) 89.
[27] P. Saul, C.R.A. Catlow, J. Kendrick, Phil. Mag. B 51 (1985) 107.
[28] P. Kofstad, Nonstoichiometry, Diffusion and Electrical Conductivity in Binary Metal Oxides, Wiley, New York, 1972.
[29] K.D. Kreuer, Chem. Mater. 8 (1996) 610.
[30] T. Norby, Y. Larring, Current Opinion in Solid State & Materials Science 2 (1997) 593.